ACS Photonics

Article

pubs.acs.org/journal/apchd5

Dynamics, Efficiency, and Energy Distribution of Nonlinear Plasmon-Assisted Generation of Hot Carriers

Olivier Demichel,* Marlène Petit, Sviatlana Viarbitskaya, Régis Méjard, Frédérique de Fornel, Edouard Hertz, Franck Billard, Alexandre Bouhelier, and Benoit Cluzel

Laboratoire Interdisciplinaire Carnot de Bourgogne, UMR 6303 CNRS-Université Bourgogne Franche-Comté, 21078 Dijon, France

Supporting Information

ABSTRACT: We employ nonlinear autocorrelation measurements to investigate plasmon-assisted hot carrier dynamics occurring in optical gold antennas. A nonlinear formation of hot carriers is produced by the excitation of surface plasmons, providing thus a unique lever to optimize the energy distribution and generation efficiency of the photoexcited charges. The temporal response of the carriers' relaxation is controlled within a range extending from 500 fs to 2.5 ps. By conducting a quantitative analysis of the dynamics, we determine the nonlinear absorption cross-section of individual optical antennas. This work sheds new insights on the understanding of plasmon-induced hot carrier generation, especially in view of applications where the time response plays a preponderant role.

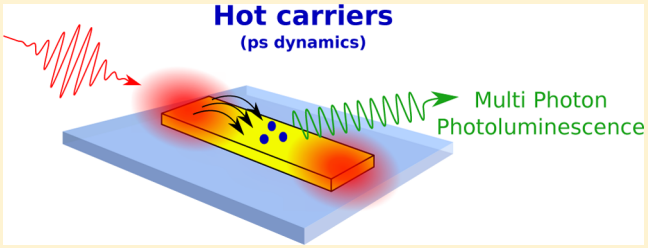

KEYWORDS: *plasmonics, hot carrier dynamics, nonlinear absorption cross-section, multiphoton luminescence*

Plasmonics—a general term associated with the collective charge oscillations induced by an electromagnetic excitation—aims at merging the ultrafast dynamics of electrons with the extreme localization of photons to open new avenues in the development of ultrafast electronics[1] or subwavelength light manipulation.[2] Surface plasmons have introduced a new paradigm in nanophotonics due to their ability to concentrate far-field radiation into nanoscale domains. Plasmonics has already penetrated a large domain of applications including single-molecule sensing,[3] photothermal cancer therapy,[4] photovoltaics,[5] and more recently hot carrier harvesting.[6]

Upon direct absorption of a photon, the electromagnetic energy is transferred to the carriers of the metal, producing pairs of out-of-equilibrium electrons and holes referred to as hot carriers. Alternatively, the electromagnetic energy may be coupled to the surface plasmons decaying either radiatively by emitting a photon in the far field or through nonradiative electronic transitions, which results in the production of hot carriers. Recent theoretical[6−8] and experimental[9] contributions demonstrated that a plasmon-assisted generation of hot carriers is much more efficient than a direct carrier photoexcitation. This makes plasmonic nanostructures a very promising venue for developing the next generation of hot carrier technologies[10,11] with already demonstrated proofs-of-concept in photochemistry,[12] photodetection,[13,14] or photocatalysis[15] to name a few. These pioneer investigations are essentially focused on the optimization of carrier harvesting through an energy level engineering and are largely leaving aside the intrinsic dynamics of the carriers. Yet, the time scales involved in hot carrier relaxation dictate the rate at which the energy is converted into heat[16−22] and play a fundamental role in determining the probability of transferring hot carriers into nearby acceptor levels or inducing chemical reactions. There are two other decisive parameters that should be optimized as well. They are the efficiency of the hot carrier generation and their energy distribution. Concerning the latter, only the decay of a single plasmon has been considered to date for a linear production of hot carriers.[6−12,14,15] The energy of the nonequilibrium distribution is then intrinsically limited by the surface plasmon energy, e.g., lower than 2.3 eV for gold-based plasmonics. As for the efficiency, hot carrier formation is dictated by the electronic density of states (eDOS). For gold, the density of electrons drastically increases at the onset of the d-bands situated at a few electronvolts below the Fermi level.[6,23] Hence, a single linear plasmon excitation process does not allow for simultaneously controlling the hot carrier efficiency and energy distribution.

In this Letter, we address these limitations by tailoring the yield, the energy distribution, and the dynamics through a nonlinear generation of photoexcited charges. Akin to a wide range of optical nonlinear effects observed in optical antennas, we benefit from the near-field electromagnetic enhancement associated with the excitation of surface plasmons.[24−27] Using autocorrelation measurements of the nonlinear photoluminescence response of an individual optical antenna,[28−30] we probe the relaxation dynamics of hot carriers produced by the participation of three plasmons. The plasmon resonance and the optical pumping power positively contribute to increase the number of carriers. We find that these parameters are also

Received: December 18, 2015
Published: April 14, 2016

DOI: 10.1021/acsphotonics.5b00726
ACS Photonics 2016, 3, 791−795

affecting the dynamics, providing thus a leverage to extend the relaxation kinetics in the 500 fs to 2.5 ps range. We further quantify the efficiency of hot carrier generation by determining the nonlinear absorption cross-section of resonant and off-resonant plasmonic antennas.

Plasmonic gold nanorod antennas are fabricated by standard electron-beam lithography followed by metal deposition and lift-off. An array of gold nanorods with a width of 55 nm and lengths varying from 90 to 800 nm and a plain thin gold film are fabricated during the same process to ensure similar material quality and a common thickness of 35 nm. Localized surface plasmon resonances of such nanoantennas were previously reported in ref 27. The dynamics is probed by multiphoton photoluminescence (MPPL) autocorrelation measurements.[28,29] A Ti:sapphire laser producing 120 fs pulses at 800 nm is focused into a diffraction-limited 300 nm spot by a high numerical aperture oil-immersion objective (60×, NA 1.49). The nanorod antennas are positioned in the focal plane of the objective. The same objective collects the blue-shifted broad nonlinear photoluminescence, which is spectrally separated from the fundamental wavelength. Autocorrelation measurements are performed with a homemade Michelson interferometer. The incident laser beam is split into two arms before being recombined and focused on a single nanoantenna. The optical path of one arm is motorized to control the interpulse delay with a femtosecond resolution. The dispersion induced along the optical path is carefully precompensated with a 4−f zero dispersion line[31] to ensure Fourier transform limited chirp-free focused optical pulses. Experiments are performed at room temperature (T_0 = 300 K).

Figure 1a sketches the plasmon-assisted MPPL mechanism in a gold nanorod and the decay of surface plasmons to hot carriers. MPPL is a nonlinear incoherent mechanism involving a sequential absorption mediated by a real intermediate state populated by hot carriers.[29] The dynamic of the response is governed by the lifetime of the intermediate state, and MPPL is thus a valuable tool to investigate plasmon-induced hot carrier generation efficiency and relaxation. Figure 1b shows the typical nonlinear emission spectrum generated by the gold film. The spectrum is limited by the transparency window of the microscope objective and by the rejecting laser line filter. The nonlinear spectrum is composed of a broadband MPPL contribution together with a coherent second-harmonic generation (SHG) at 400 nm. The electronic DOS for Au is depicted in Figure 1c. The number of vertical arrows for a given transition represents the order of the nonlinear process, and the length of the arrows corresponds to the laser energy (1.55 eV). The Fermi level defines the origin of the energy scale. Fermi's golden rule says that the electronic transition rate is proportional to the joint electronic DOS of electrons and holes, which is minimal for the case of a single plasmon decay (one arrow). On the contrary, the decay of three or four plasmons is much more favored owing to the high density of states available in the d-bands. Then, a single plasmon excitation near the Fermi level decaying in hot carriers is less efficient compared to higher order plasmon processes. In line with this argument, Figure 2a shows an MPPL nonlinearity order close to 4, as already reported by Biagioni.[29] The SHG nonlinearity is about 2, the noninteger value is due to the residual MPPL contribution overlapping the SHG peak (see spectra of Figure 1b). The plasmon-induced hot carriers generated by the process can potentially reach energies as high as 4 × 1.5−6 eV. Despite a four-photon-mediated photo-

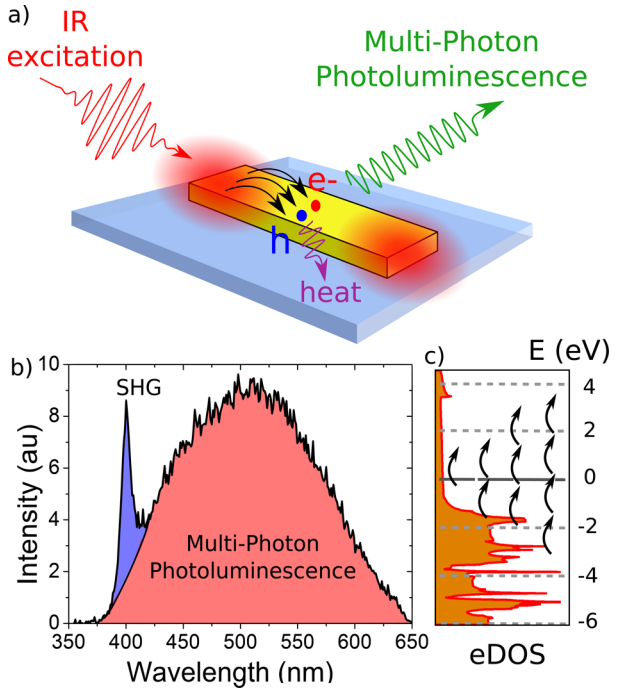

Figure 1. (a) Schematic view of the nonlinear plasmon-induced generation of hot carriers producing multiphoton photoluminescence (MPPL). (b) Typical nonlinear emission spectrum of a thin gold film featuring the SHG at 400 nm and the broad band MPPL signal. (c) Representation of the gold's electronic DOS. The arrows indicate transitions assisted with respectively 1 to 4 plasmons.

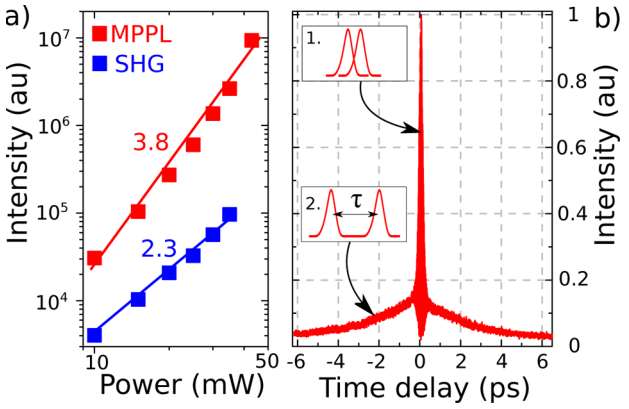

Figure 2. (a) Power dependence of SHG and MPPL intensity. (b) MPPL autocorrelation measurement from a gold nanorod. For short interpulse delay (inset 1), the two pulses temporally overlap on the antenna, resulting in an interference pattern. Longer delays reveal the dynamics of the MPPL intensity decay (inset 2).

luminescence, no signal can be recorded below 370 nm in our experimental setup because of the cutoff of our CCD camera and of the laser line filters and the large imaginary component of the Au's dielectric function in these wavelengths.

Figure 2b illustrates a typical MPPL autocorrelation trace measured from a gold nanorod. In the region where pulses overlap (inset 1), interferences are driving the MPPL intensity, hiding thus its ultrafast dynamics. In the following, we consider only a delay longer than 450 fs when pulses are not temporally overlapping (inset 2). In this regime, the MPPL signal decreases exponentially with the interpulse delay. These wings indicate that the MPPL is a two-step mechanism

DOI: 10.1021/acsphotonics.5b00726
ACS Photonics 2016, 3, 791−795

involving an intermediate state with a finite lifetime, and the exponential decay probes this lifetime. In our hot carrier description of the MPPL mechanism, the first and the second pulse generate a distribution of hot carriers recombining by emitting photons. However, the first pulse also populates the latter intermediate state with hot carriers, which relax through carrier−phonon interactions. Then, for interpulse delays shorter than the hot carrier relaxation time, plasmons generated by the second pulse can also decay by transferring their energy to these hot carriers produced by the first pulse. Re-excited carriers may then recombine radiatively. The MPPL autocorrelation traces probe the dynamics of the carrrier−phonon interactions.[16−18] Note that the slight asymmetry in the autocorrelation trace comes from a slight difference of power between both pulses. For the sake of accuracy we consider only the right part of the traces in the following.

We now turn to the fundamental question addressed in this work: can one control plasmon-induced hot carrier dynamics? The nonlinear process creating the hot carrier population is strongly affected by the local electromagnetic field enhancement. Hence, the generation efficiency can be independently optimized by shaping the geometry of the nanorod. We thus investigate the influence of plasmon resonances by probing the hot carrier lifetime for the fabricated array of gold nanoantennas with varying lengths. Figure 3a and b show the MPPL intensity and hot carrier relaxation time as a function of the nanorod length L, respectively. There are two resonances revealed by the MPPL signal corresponding to the first two

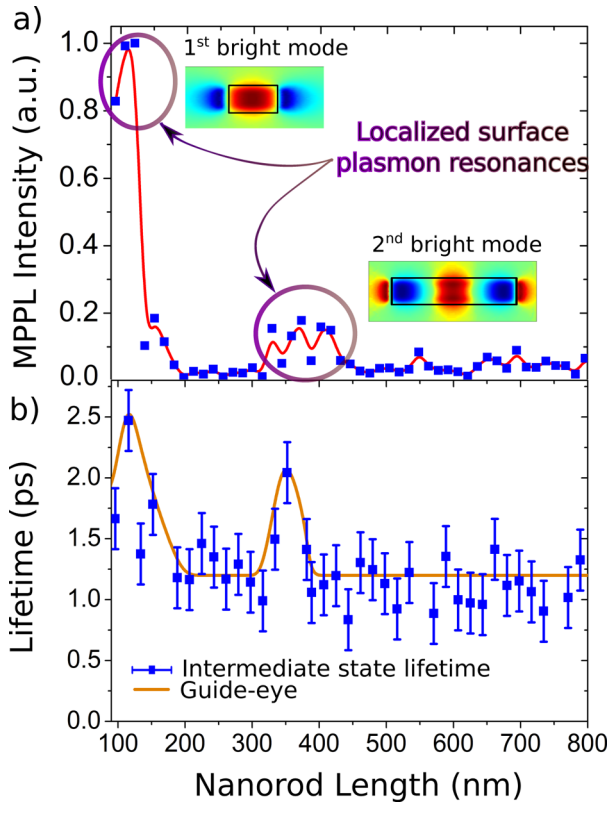

Figure 3. (a, b) Evolution of the MPPL intensity and the intermediate state lifetime with the length of the nanorods, respectively. Insets: Finite element numerical simulation of the electric field distribution parallel to the nanorod for L = 100 nm and L = 360 nm. The red line of panel (a) is an average of three consecutive data points.

bright plasmon modes.[27] The electric field distributions of the antenna excited by a focused laser beam are simulated by a finite-element method. The electric field component parallel to the long axis of the nanorod is reported in the inset of Figure 3a. We computed the spectral dependence of near-field intensity as a function of the nanorod lengths. These spectra confirm the spectral position of plasmonic resonances (see Supporting Information). A clear correlation exists between the MPPL intensity and the relaxation dynamics. The relaxation time is 1.25 ± 0.25 ps for every off-resonant nanorod, whereas the dynamics for resonant antennas are enhanced by a factor of 2, reaching up to 2.5 ± 0.25 ps. Hence, by engineering the plasmon response of the antennas, the hot carrier lifetimes can be readily controlled.

To provide a deeper understanding, we provide in the following a description of hot carrier dynamics. Immediately after the decay of the plasmons into hot carriers, the energy of photoexcited charges has a Dirac distribution that is then redistributed by carrier−carrier interactions following an internal thermalization process extensively discussed in ref 19. After this fast relaxation, experimentally hidden within the region where pulses interfere, the carrier distribution is described by an electronic temperature $T_{e,0}$.[16−18] The carriers are then relaxing down to the Fermi level by transferring their energy to the lattice. Their energy distribution narrows, and the associated electronic temperature (T_e) decreases progressively.[16−19] The process is generally described in the framework of the two-temperature model defined by the rate equation[19]

$$C_e \frac{dT_e}{dt} = -\Gamma_{e,ph}(T_e - T_0) \quad (1)$$

where $\Gamma_{e,ph}$ is the carrier−phonon coupling constant. The initial electronic capacity is defined as $C_e = c_o T_{e,0}$ in the weak perturbation approximation[19] available here since the hot carrier dynamics always follows a single-exponential decay. c_o is the Sommerfeld constant. According to that model, the hot carrier lifetime τ_e is written as[19,20]

$$\tau_e = \frac{c_0 T_{e,0}}{\Gamma_{e,ph}} = \frac{c_0}{\Gamma_{e,ph}} \sqrt{T_0^2 + \frac{2u_{abs}}{c_0}} \quad (2)$$

where the initial temperature $T_{e,0}$ is expressed as a function of the room temperature (T_0) and the energy absorbed per unit volume within a pulse (u_{abs}). The presence of T_0 in eq 2 originates from the fact that before the impulse excitation, and also for low illuminating power, $T_{e,0} = T_0$, in agreement with refs 16−19. The electronic temperature then increases with the number of generated carriers, which produce stronger electron−electron interactions. This simple two-temperature model does not take into account any direct dependence on surface plasmons. Nevertheless, the term u_{abs} results from the product of the photon flux with the effective absorption cross-section of the nanorod, which is increased at resonance.[32,33] In other words, the two-temperature model indirectly describes the plasmon dependence of the hot carrier dynamics.

According to eq 2, τ_e depends only on the absorbed energy per pulse (u_{abs}) since other parameters are the lattice temperature and the properties of the material. Hence, the lifetime of the hot carrier distribution must depend on the excitation power. We quantitatively compare in the following the power dependence for structures having different absorption cross sections. Figure 4 display the dynamics for a 100 nm long resonant antenna (blue squares), a 500 nm long

DOI: 10.1021/acsphotonics.5b00726
ACS Photonics 2016, 3, 791−795

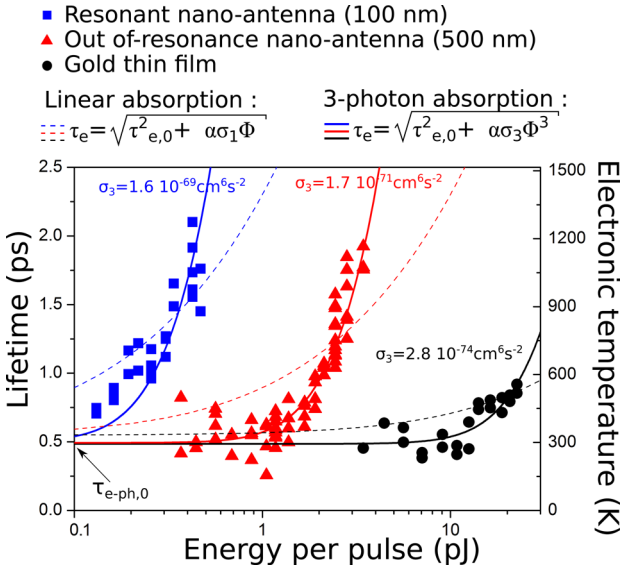

Figure 4. Evolution of the intermediate lifetime τ_e with the pulse energy for a resonant antenna (blue squares), an out-of-resonance antenna (red triangles), and a planar gold thin film (dark circles). Solid and dashed colored lines correspond to simulations based on the two-temperature model, assuming that the intermediate state results respectively from a single or a three-photon absorption.

off-resonant nanorod (red triangles), and a planar thin film (black dots) as a function of the pulse energy. Regardless of the type of structures, the lifetime is about 500 fs for low pulse energies. For gold, c_0 = 66 J m^{-3} K^{-2}[34] and $\Gamma_{e,ph}$ = 4 × 10^{16} W m^{-3} K^{-1};[16] thus in the low-excitation regime, the thermalization time is given by $\tau_{e,0} = \frac{c_0 T_0}{\Gamma_{e,ph}}$ = 495 fs, in good agreement with our measurements. This value is consistent with the literature reporting hot carrier dynamics in the 0.5−4 ps range, irrespective of the nonlinearity order of the MPPL process.[19,20,28−30] For higher pulse energy, u_{abs} increases, and in agreement with eq 2, we observe a concomitant rise of the lifetime. The evolution with the pulse energy underpins a dynamic governed by carrier−phonon interactions with a time scale directly related to the electron temperature after internal thermalization, $T_{e,0}$. The latter is readily inferred by feeding τ_e in eq 2 and is reported on the right axis of Figure 4.

Figure 4 shows that the dynamics of the thin film starts to be sensitive to the excitation power for a pulse energy 2 orders of magnitude higher than for a resonant nanorod. This is understood from the enhancement of the absorption cross-section at resonance. The dashed lines plotted in Figure 4 are the best fits to the experimental data assuming that the hot carriers are generated by a linear absorption. A single-plasmon process is clearly not reproducing the experimental trends. A better match to the data is obtained from a cubic dependence of u_{abs} on the pulse energy, as shown by the solid lines of Figure 4. We conclude that three plasmons are needed to populate the intermediate state with hot carriers after the first pulse, the second pulse providing only a fourth plasmon to the hot carrier distribution in agreement with the order of the MPPL nonlinearity (Figure 2a). The absorbed energy per pulse delivered in the system is written as $u_{abs} = 3\sigma_3 h\nu\tau\Phi^3$, where σ_3 refers to the three-photon absorption cross-section, $h\nu$ and Φ are respectively the photon energy and flux, and τ is the pulse duration. From the fits of Figure 4, we quantitatively evaluate σ_3 for the two antennas and the thin film. We find σ_3 = 2.8 × 10^{-74} cm^6 s^2 photon^{-2} for the gold thin film, σ_3 = 1.7 × 10^{-71} cm^6 s^2 photon^{-2} for the nonresonant antenna, and σ_3 = 1.6 × 10^{-69} cm^6 s^2 photon^{-2} for the resonant antenna. To our knowledge, these values are the first estimates for the three-photon absorption cross-section of gold nanostructures. Although the Gaussian optical illumination is not uniform along antennas (especially for the 500 nm one) and the absorption cross-section could be slightly underestimated, these numbers are orders of magnitude higher than those of single molecules and semiconductor nanoparticles, which are respectively about 10^{-80} cm^6 s^2 photon^{-2} [35] and in the 10^{-75}−10^{-79} cm^6 s^2 photon^{-2} range.[36] Note that the absorption cross-section of the 500 nm long antenna could be slightly underestimated because the antenna is not strictly covered by the diffraction-limited spot.

In conclusion, we investigated the hot carrier dynamics generated in Au optical antennas through a plasmon-assisted mechanism. We found that the mediation of surface plasmons is essential to optimize the nonlinear generation of hot carriers. Specifically, through an increased optical absorption cross-section at the antenna's resonance, the efficiency of the hot carrier generation increases by 100-fold compared to off-resonances and by 10^5 compared to thin films. The electronic temperature can be elevated above 1000 K, providing thus an enlarged energy distribution. We further demonstrate that the resonance and the light power both retard the ultrafast relaxation of the photoexcited charges to the phonon bath and can be as long as a few picoseconds, allowing for a control of the hot carrier dynamics. Finally, we determined the nonlinear absorption cross-section of various plasmonic structures based on a quantitative analysis of the evolution of the relaxation dynamics with the incident pulse energy. Adjusting the different levers controlling the intrinsic properties of hot carriers (excitation efficiency, energy distribution, and dynamics) and quantifying the relevant absorption cross-sections are of crucial importance for advancing the next generation of plasmon-assisted hot carrier applications such as photochemistry, photodetection, or photocatalysis.

■ ASSOCIATED CONTENT

Supporting Information

The Supporting Information is available free of charge on the ACS Publications website at DOI: 10.1021/acsphotonics.5b00726.

Additonal information (PDF)

■ AUTHOR INFORMATION

Corresponding Author

*E-mail: olivier.demichel@u-bourgogne.fr.

Notes

The authors declare no competing financial interest.

■ ACKNOWLEDGMENTS

The research leading to these results has received funding from the European Research Council under the European Community's Seventh Framework Program FP7/20072013 Grant Agreement no. 306772 as well as the Agence Nationale de la Recherche (grants PLACORE ANR-13-BS10-0007 and CoConicS ANR-13-BS08-0013). This project has been performed in cooperation with the Labex ACTION program (contract ANR-11-LABX-0001-01). O.D. and M.P. thank D.

DOI: 10.1021/acsphotonics.5b00726
ACS Photonics 2016, 3, 791−795

Thao for fruitful discussions, and the authors thanks V. Meunier for eDOS computations.

REFERENCES

(1) Ozbay, E. Plasmonics: Merging Photonics and Electronics at Nanoscale Dimensions. *Science* **2006**, *311*, 189−193.
(2) Barnes, W. L.; Dereux, A.; Ebbesen, T. W. Surface plasmon subwavelength optics. *Nature* **2003**, *424*, 824−830.
(3) Xu, H.; Bjerneld, E. J.; Käll, M.; Börjesson, L. Spec-troscopy of Single Hemoglobin Molecules by Surface Enhanced Raman Scattering. *Phys. Rev. Lett.* **1999**, *83*, 4357−4360.
(4) Loo, C.; Lowery, A.; Halas, N.; West, J.; Drezek, R. Immunotargeted Nanoshells for Integrated Cancer Imaging and Therapy. *Nano Lett.* **2005**, *5*, 709−711.
(5) Atwater, H. A.; Polman, A. Plasmonics for improved photovoltaic devices. *Nat. Mater.* **2010**, *9*, 205−213.
(6) Sundararaman, R.; Narang, P.; Jermyn, A. S.; Goddard, W. A., III; Atwater, H. A. Theoretical predictions for hot-carrier generation from surface plasmon decay. *Nat. Commun.* **2014**, *5*, 5.
(7) Manjavacas, A.; Liu, J. G.; Kulkarni, V.; Nordlander, P. Plasmon-Induced Hot Carriers in Metallic Nanoparticles. *ACS Nano* **2014**, *8*, 7630−7638.
(8) Zhang, H.; Govorov, A. O. Optical Generation of Hot Plasmonic Carriers in Metal Nanocrystals: The Effects of Shape and Field Enhancement. *J. Phys. Chem. C* **2014**, *118*, 7606−7614.
(9) Zheng, B. Y.; Zhao, H.; Manjavacas, A.; McClain, M.; Nordlander, P.; Halas, N. J. Distinguishing between plasmon-induced and photoexcited carriers in a device geometry. *Nat. Commun.* **2015**, *6*, 6.
(10) Brongersma, M. L.; Halas, N. J.; Nordlander, P. Plasmon-induced hot carrier science and technology. *Nat. Nanotechnol.* **2015**, *10*, 25−34.
(11) Clavero, C. Plasmon-induced hot-electron generation at nanoparticle/metal-oxide interfaces for photovoltaic and photo-catalytic devices. *Nat. Photonics* **2014**, *8*, 95−103.
(12) Takahashi, Y.; Tatsuma, T. Solid state photovoltaic cells based on localized surface plasmon-induced charge separation. *Appl. Phys. Lett.* **2011**, *99*, 182110.
(13) Stolz, A.; Berthelot, J.; Mennemanteuil, M.-M.; des Francs, G. C.; Markey, L.; Meunier, V.; Bouhelier, A. Nonlinear Photon-Assisted Tunneling Transport in Optical Gap Antennas. *Nano Lett.* **2014**, *14*, 2330−2338.
(14) Sobhani, A.; Knight, M. W.; Wang, Y.; Zheng, B.; King, N. S.; Brown, L. V.; Fang, Z.; Nordlander, P.; Halas, N. J. Photodetection with Active Optical Antennas. *Nat. Commun.* **2013**, *4*, 1643.
(15) Mubeen, S.; Lee, J.; Singh, N.; Kramer, S.; Stucky, G. D.; Moskovits, M. An autonomous photosynthetic device in which all charge carriers derive from surface plasmons. *Nat. Nanotechnol.* **2013**, *8*, 247−251.
(16) Fann, W. S.; Storz, R.; Tom, H. W. K.; Bokor, J. Electron thermalization in gold. *Phys. Rev. B: Condens. Matter Mater. Phys.* **1992**, *46*, 13592−13595.
(17) Groeneveld, R. H. M.; Sprik, R.; Lagendijk, A. Femtosecond spectroscopy of electron-electron and electronphonon energy relaxation in Ag and Au. *Phys. Rev. B: Condens. Matter Mater. Phys.* **1995**, *51*, 11433−11445.
(18) Sun, C.-K.; Vallée, F.; Acioli, L. H.; Ippen, E. P.; Fujimoto, J. G. Femtosecond-tunable measurement of electron thermalization in gold. *Phys. Rev. B: Condens. Matter Mater. Phys.* **1994**, *50*, 15337−15348.
(19) Del Fatti, N.; Voisin, C.; Achermann, M.; Tzortzakis, S.; Christofilos, D.; Vallée, F. Nonequilibrium electron dynamics in noble metals. *Phys. Rev. B: Condens. Matter Mater. Phys.* **2000**, *61*, 16956−16966.
(20) Baida, H.; Mongin, D.; Christofilos, D.; Bachelier, G.; Crut, A.; Maioli, P.; Del Fatti, N.; Vallée, F. Ultrafast Nonlinear Optical Response of a Single Gold Nanorod near Its Surface Plasmon Resonance. *Phys. Rev. Lett.* **2011**, *107*, 057402.
(21) Huang, J.; Wang, W.; Murphy, C. J.; Cahill, D. G. Resonant secondary light emission from plasmonic Au nanostructures at high electron temperatures created by pulsed-laser excitation. *Proc. Natl. Acad. Sci. U. S. A.* **2014**, *111*, 906−911.
(22) Harutyunyan, H.; Martinson, A. B. F.; Rosenmann, D.; Khorashad, L. K.; Besteiro, L. V.; Govorov, A. O.; Wiederrecht, G. P. Anomalous ultrafast dynamics of hot plasmonic electrons in nanostructures with hot spots. *Nat. Nanotechnol.* **2015**, *10*, 770−774.
(23) Lässer, R.; Smith, N. V.; Benbow, R. L. Empirical band calculations of the optical properties of *d*-band metals. I. Cu, Ag, and Au. *Phys. Rev. B: Condens. Matter Mater. Phys.* **1981**, *24*, 1895−1909.
(24) Bouhelier, A.; Beversluis, M.; Novotny, L. Characterization of nanoplasmonic structures by locally excited photoluminescence. *Appl. Phys. Lett.* **2003**, *82*, 4596.
(25) Imura, K.; Nagahara, T.; Okamoto, H. Near-Field Two-Photon-Induced Photoluminescence from Single Gold Nanorods and Imaging of Plasmon Modes. *J. Phys. Chem. B* **2005**, *109*, 13214−13220.
(26) Kauranen, M.; Zayats, A. V. Nonlinear plasmonics. *Nat. Photonics* **2012**, *6*, 737−748.
(27) Demichel, O.; Petit, M.; des Francs, G. C.; Bouhelier, A.; Hertz, E.; Billard, F.; de Fornel, F.; Cluzel, B. Selective excitation of bright and dark plasmonic resonances of single gold nanorods. *Opt. Express* **2014**, *22*, 15088−15096.
(28) Biagioni, P.; Celebrano, M.; Savoini, M.; Grancini, G.; Brida, D.; Mátéfi-Tempfli, S.; Mátéfi-Tempfli, M.; Duò, L.; Hecht, B.; Cerullo, G.; et al. Dependence of the two-photon photoluminescence yield of gold nanostructures on the laser pulse duration. *Phys. Rev. B: Condens. Matter Mater. Phys.* **2009**, *80*, 045411.
(29) Biagioni, P.; Brida, D.; Huang, J.-S.; Kern, J.; Duò, L.; Hecht, B.; Finazzi, M.; Cerullo, G. Dynamics of Four-Photon Photoluminescence in Gold Nanoantennas. *Nano Lett.* **2012**, *12*, 2941−2947.
(30) Jiang, X.-F.; Pan, Y.; Jiang, C.; Zhao, T.; Yuan, P.; Venkatesan, T.; Xu, Q.-H. Excitation Nature of Two-Photon Photoluminescence of Gold Nanorods and Coupled Gold Nanoparticles Studied by Two-Pulse Emission Modulation Spectroscopy. *J. Phys. Chem. Lett.* **2013**, *4*, 1634−1638.
(31) Weiner, A. M. Ultrafast optical pulse shaping: A tutorial review. *Opt. Commun.* **2011**, *284*, 3669−3692.
(32) Pelton, M.; Aizpurua, J.; Bryant, G. Metal-nanoparticle plasmonics. *Laser Photonics Rev.* **2008**, *2*, 136−159.
(33) Derom, S.; Vincent, R.; Bouhelier, A.; Colas des Francs, G. Resonance quality, radiative/ohmic losses and modal volume of Mie plasmons. *EPL* **2012**, *98*, 47008.
(34) Sun, C.-K.; Vallée, F.; Acioli, L.; Ippen, E. P.; Fujimoto, J. G. Femtosecond investigation of electron thermalization in gold. *Phys. Rev. B: Condens. Matter Mater. Phys.* **1993**, *48*, 12365−12368.
(35) Liu, J.; Li, G.; Wang, Y. Impact of Electron Acceptor on Three-Photon Absorption Cross-Section of the Fluorene Derivatives. *J. Phys. Chem. A* **2012**, *116*, 7445−7451.
(36) Xing, G.; Chakrabortty, S.; Ngiam, S. W.; Chan, Y.; Sum, T. C. Three-Photon Absorption in Seeded CdSe/CdS Nanorod Hetero-structures. *J. Phys. Chem. C* **2011**, *115*, 17711−17716.

DOI: 10.1021/acsphotonics.5b00726
ACS Photonics 2016, 3, 791−795